IEEE Access
Multidisciplinary | Rapid Review | Open Access Journal

Received December 3, 2020, accepted December 30, 2020, date of publication January 11, 2021, date of current version January 20, 2021.

Digital Object Identifier 10.1109/ACCESS.2021.3050651

On Two Algorithms for Multi-Modality Image Registration Based on Gaussian Curvature and Application to Medical Images

NASRA BEGUM[1], NOOR BADSHAH[1], MAZLINDA IBRAHIM[2], MUNIBA ASHFAQ[3], NASRU MINALLAH[3], AND HADIA ATTA[4]

[1]Department of Basic Sciences, University of Engineering and Technology, Peshawar, Peshawar 25120, Pakistan
[2]Department of Mathematics, National Defense University of Malaysia (UPNM), Kuala Lumpur 57000, Malaysia
[3]Department of Computer Systems Engineering, University of Engineering and Technology, Peshawar, Peshawar 25120, Pakistan
[4]Department of Mathematics, Islamia College Peshawar, Peshawar 25120, Pakistan

Corresponding author: Noor Badshah (noor2knoor@gmail.com)

ABSTRACT Registration of multi-modal images is one of the challenging problems in image processing nowadays. In this paper, two novel non-rigid registration models are proposed for multi-modality images. In model 1, mutual information of the template and reference images is used as data fitting term with Gaussian curvature regularization. This approach may not give satisfactory results in noisy images or images having bias field. To overcome this drawback, model 2 is proposed which is based on normalized gradient of both template and reference images as a data fitting term instead of mutual information. To get best transformations, both the models are minimized by using Augmented Lagrangian Method. The proposed models can register multi-modality images without effecting edges and other important fine details and are also tested on various medical images like (T1-T2 MRI, PD weighted-T2 MRI) noisy and synthetic images. The proposed models are also tested on a well known free available Brainweb dataset, where they produced satisfactory results. From experimental results, it can be observed that normalized gradient field based model gives better results than mutual information based model. Comparison is done qualitatively and quantitatively through Jaccard Similarity Coefficient.

INDEX TERMS Image registration, multi-modality images, Gaussian curvature (GC), mutual information (MI), normalized gradient field (NGF), T1-T2 MR images, PD weighted MRI, bias field, augmented Lagrangian method (ALM), Jaccard similarity coefficient (JSC).

I. INTRODUCTION

Image registration is one of the most important and challenging task in medical imaging, which aims on finding an optimal transformation for alignment of different images data. Image registration is widely used in art, astronomy, criminology, cartography, computer vision, biological imaging, remote sensing and especially in medical imaging for diagnosis,monitoring of tumor growth and for therapy guidance [1]–[5].

General Frame Work: For given template image T and reference image R, defined on $\Omega \subseteq \mathbb{R}^d$, $d \in N$ is the dimensionality of the data with smooth boundary $\partial\Omega$. In this paper $d = 2$ is used and can be generalized to other values of d.

The associate editor coordinating the review of this manuscript and approving it for publication was Trivikram Rao Molugu.

The basic idea of image registration is to find a transformation $\Phi(\mathbf{u})(\cdot) : \Omega \to \Omega$ such that $\Phi(\mathbf{u}(\mathbf{x})) = x + \mathbf{u}(\mathbf{x})$. To find this, it is enough to find a deformation or displacement field $\mathbf{u} : \Omega \to \Omega$ such that the transformed template image

$$T(\Phi(\mathbf{u}(\mathbf{x}))) = T(x + \mathbf{u}(\mathbf{x})) = T(\mathbf{u}). \tag{1}$$

becomes similar to the reference image R. Finding $\mathbf{u}(\mathbf{x}) = (u_1, u_2)$ from (1) is an inverse problem, which is usually modeled in the following way:

$$\min_{\mathbf{u}} \mathcal{J}_\alpha(\mathbf{u}) = \mathcal{D}(T(\mathbf{u}), R) + \alpha\mathcal{S}(\mathbf{u}), \tag{2}$$

This model may be used for registration of both mono-modality and multi-modality images. In (2), the first term $\mathcal{D}(T(\mathbf{u}), R)$ is a fidelity term which measure distance or similarity between the transformed template image $T(\mathbf{u})$ and the reference image R. The second term $\mathcal{S}(\mathbf{u})$ is a

regularization term which controls the smoothness of the deformation field and imparts reasonable transformations and $\alpha > 0$ is a trade-off parameter. Regularization term in inverse problem is always important and challenging and can make a model more efficient. Some of the well known regularization terms are diffusion based [6], [7], total variation based [8], [9], elastic based [10] (low order models) and curvature based [11], non-linear mean curvature based [12], linear curvature based [13] and Gaussian curvature based [14] (higher order models).

In mono-modality images, where the intensity ranges are same and have similar features, either the L^1-distance or L^2-distance (sum of square differences (SSD)) between the transformed template and reference images i.e. $\mathcal{D} = \int_\Omega (T(\mathbf{u}) - R)^2 \, d\Omega$ may be used as similarity measures. However SSD is widely used similarity measure for mono-modality images. Whereas in multi-modality image registration, the intensity ranges in the template image T and the reference image R are not directly comparable i.e. only the pattern of both images have some resemblance to each other, not their intensities. That is why, intensities of the same object in different images are not similar which makes the registration of multi-modality images a much difficult task, than the mono-modality case. Thus, the sum of squared differences and many other models in [15] for mono-modal images and the more effective technique of optimal transport in [16] cannot be used for multi-modality images.

Many intensity based similarity measures have been proposed in the field of multi-modality image registration. The well known similarity measures are Renyi entropy [17], Kullback-Leibler divergence [18], commutative residual entropy [19], normalized mutual information [20], [21] and mutual information [22]. Among all these similarity measures, mutual information (MI) is a frequently used similarity measure for multi-modal image registration [23], [24]. Another similarity measure for multi-modality image registration is normalized gradient field (NGF) [15], [25] which is based on the gradients of the transformed template and reference images and are therefore essentially intensity independent. NGF and MI as similarity measures combined with fluid registration model are used for DCE-MRI time series motion correction [26]. In [27], Chen *et al.* proposed a cross-correlation similarity measure primarily based on reproducing kernel Hilbert spaces and observed its advantages over mutual information. In [28] Ibrahim and Chen proposed a decomposition model for parametric and non-parametric image registration using MI and NGF as similarity measures and linear curvature as regularizer for multi-modality image registration. In [29], the author used the S_qN distance measure for investigation on different singular based measures of an image feature array for multi-modal images. Recently, in [30], Theljani *et al.* proposed a variational model in which they combine the two measures i.e. the normalized gradients of the images and the higher-order derivatives of the displacement filed as the fidelity and the regularizer terms respectively.

In this paper, two novel non-rigid image registration models are proposed based on Gaussian curvature of surface induced by the displacement field as regularization, and MI and NGF as similarity measures for the alignment of multi-modality images. Gaussian curvature preserves important structures such as edges and corners and also structures with low gradients. To the best of our knowledge this is for the first time that Gaussian curvature is used as regularization term with MI and NGF similarity measure. The first approach may not give satisfactory results in noisy images or images having bias field. To circumvent this problem our second model is proposed based on NGF which incorporates co-aligned gradient vectors of the corresponding images and is therefore essentially intensity independent, which leads to good registration results over rest of the model. To get best transformations, both proposed models are minimized by using Augmented Lagrangian method (ALM). The proposed models works better for large and smooth deformations without mesh folding. Also they register multi-modality images without effecting their edges and other important fine details. Motivated by the notable advantages of the proposed models, they are tested on various medical images like (T1-T2 MRI, PD weighted-T2 MRI) noisy and synthetic images. The proposed models are also tested on a well known free available Brainweb data set, where they produced satisfactory results. From the experimental results, it can be observed that NGF based model 2 gives better results than MI based model. The proposed models are also compared with two other state-of-the-art models which produce better results than the existing models (where the existing models uses linear curvature may not produce better results for large deformations and may produce mesh folding). Also the comparison between the proposed models are done by adding the Gaussian noise to MR image of TEST 1, which shows that the proposed model using NGF can efficiently work. Comparison is done qualitatively and quantitatively through Jaccard Similarity Coefficient (JSC) and also evaluate the accuracy by correlation coefficient between the reference and template images.

The rest of the paper is organized as follows: The proposed models are explained in section II-C. The numerical solution of the proposed models by Augmented Lagrangian method is given in section III. Section IV is dedicated to the implementation of numerical experiments to check the efficiency and robustness of the models. Finally, the conclusion is given in section V.

II. METHODOLOGIES

General framework of registration models is based on similarity measures and regularization. Here a brief discussion is given about similarity measures and regularization, which are used in development of the proposed model for registration of multi-modal images.

A. CHOICE OF SIMILARITY MEASURES

The image similarity measure plays an important role to determine the correlation between two images in order to

quantify the quality of image registration. The selection of the image similarity measure requires a trade-off between speed and performance. Registration of multi-modality images requires similarity measures that can deal with complex and unknown image intensity dependencies. Such measures have to rely on statistics, and consequently, they require relatively large image regions to operate. Here a brief discussion is given about similarity measures, which are used in proposed models.

1) MUTUAL INFORMATION (MI)

Intensities of two images may be compared through similarity measures which uses statistical or information theory [31]. Mutual information was introduced by Viola and Wells III [24] for registration of multi-modality images, which may be defined as:

$$\mathcal{MI}(R, T) = H(R) + H(T) - H(R, T), \tag{3}$$

where $H(R), H(T)$ denotes the marginal entropy and $H(R, T)$ is the joint entropy of random variables R, T respectively. The analogous to the Kullback-Leibler measure [32], the mutual information of random variables R and T is defined as:

$$\mathcal{MI}(R, T) = \sum_{s,t} p^{(R,T)}(s, t) \log \frac{p^{(R,T)}(s, t)}{p^{(R)}(s)p^{(T)}(t)}, \tag{4}$$

where $p^{(R,T)}(s, t)$ and $p^{(R)}(s), p^{(T)}(t)$ represents the joint and marginal probability distributions of image R and T respectively.

In [31], mutual information based on differential entropy is used. The mutual information of two images is maximal when they are geometrically aligned [33] and it measures how the intensity distribution of two images fails to be independent. The mutual information as similarity measure [34], [35] is given as

$$\mathcal{D}^{\mathcal{MI}}(T(\mathbf{u}), R) = -\int_{\mathbb{R}^2} p^{T(\mathbf{u}),R}(t, s) \log \frac{p^{T(\mathbf{u}),R}(t, s)}{p^{T(\mathbf{u})}(t)p^{R}(s)} dtds. \tag{5}$$

where the probability density function $p^{T}(t)$ can be estimated by using Parzen window [37], [38] and is given by:

$$p^{(T)}(t) = \frac{1}{N} \sum_{j=1}^{N} \frac{g_k((t - t_j)/\sigma)}{\sigma}, \tag{6}$$

where $\{t_j\}$ be a set of N samples of random variable T (given image) with probability density function $p^{(T)}(t)$. Also g_k is the kernel function such that $\int g_k(t)dt = 1$ and the parameter σ is the width of the parzen window kernel. In [15], g_k is used as cubic spline kernel for estimating the joint pdf with $\sigma = 1$ and is given as:

$$g_k(t) = \begin{cases} (t+2)^3, & -2 \le t < -1 \\ -t^3 - 2(t+1)^3 + 6(t+1), & -1 \le t < 0 \\ t^3 + 2(t-1)^3 - 6(t-1), & 0 \le t < 1 \\ (2-t)^3, & 1 \le t < 2 \\ 0, & elsewhere. \end{cases}$$

For other possibilities of $g_k(t)$ see [39]. In next section, a brief discussion is given about the other similarity measure.

2) NORMALIZED GRADIENT FIELD (NGF)

The sum of squared distance measure can be used for images R and $T(\mathbf{u})$ of same modalities, whereas mutual information (MI) is an alternative similarity measure for multi-modality images with assumption that R and $T(\mathbf{u})$ are statistically dependent. These measures may not produce good results in aligning edges in the images. The normalized gradient field (NGF), which uses gradient of the images. The normalized gradient field (NGF) is used for the alignment of the edges in the reference image R and transformed template image $T(\mathbf{u})$. Consider the following normalized gradient field:

$$nT(\mathbf{u}) = \frac{\nabla T(\mathbf{u})}{\sqrt{\|\nabla T(\mathbf{u})\|_2^2 + \eta^2}} = \frac{\nabla T(\mathbf{u})}{\|\nabla_\eta T(\mathbf{u})\|},$$
$$nR = \frac{\nabla R}{\sqrt{\|\nabla R\|_2^2 + \eta^2}} = \frac{\nabla R}{\|\nabla_\eta R\|}, \tag{7}$$

where η is the edge parameter that controls the influence of image gradient, and here it controls the singularity problem, which can be computed as [25], [40]:

$$\eta = \frac{\xi}{\mathcal{V}} \int_\Omega |\nabla T(\mathbf{u})| d\Omega, \tag{8}$$

where ξ is the estimated noise level and $\mathcal{V}$ is the cardinal number associated with domain. The parameter η can be taken as threshold for identification of edges in an image. When η is less than norm of the gradient of image, then the feature will be considered as an edge and if η is greater than norm of the gradient, the feature will be considered as noise.

The normalized gradient field distance measure for the registration of images is as follows:

$$\mathcal{D}^{ngf}(T(\mathbf{u}), R) = \int_\Omega \left(1 - \left(\left(nT(\mathbf{u})\right)^t \cdot nR\right)^2\right) d\Omega. \tag{9}$$

As the proposed models are compared with two linear curvature models [25], [45] for which the linear curvature regularizer is given in section B.

B. FICHER AND MODERSITZKI's LINEAR CURVATURE

Ficher and Modersitzki proposed the first second order regularization term for image registration as follows:

$$\mathcal{S}^{\mathrm{LC}}(\boldsymbol{u}) = \int_\Omega \left[(\Delta u_1)^2 + (\Delta u_2)^2\right] d\Omega. \tag{10}$$

The Euler Lagrange equation for (2) with S^{LC} as the regularisation term is given by:

$$\alpha \Delta^2 u + f(u) = 0 \tag{11}$$

with the boundary conditions $\Delta u_m = 0, \nabla \Delta u_m \cdot \hat{\boldsymbol{n}} = 0$, $m = 1, 2$ and $\hat{n}$ the unit outward normal vector. This model consists of the second order derivative information of the displacement field which results in smoother deformations as

compared to first order models but this may not work in large deformations. Due to the affine kernal, this model does not require affine linear pre-registration step.

In the next section, a detailed discussion is given on our novel proposed models for registration of multi-modality images.

C. THE PROPOSED MULTI-MODALITY IMAGE REGISTRATION MODELS

In this section, the first proposed model is based on mutual information as similarity measure and Gaussian curvature as regularization term, while the second model is based on normalized gradient field as similarity measure combined with Gaussian curvature as a regularization term. These models are used for non-rigid registration of multi-modality images. Let the displacement field between the reference image R and the template image T be the surface map $(x, y) :\rightarrow (x, y, u_m(x, y))$ where $m = 1, 2$ and with $\mathbf{u} = (u_1, u_2)$. We propose the following functionals for minimization to register two multi-modality images:

Energy Functional 1*:* The energy functional for our first new proposed model is based on mutual information (MI) as similarity measure and Gaussian curvature as regularization term. Mutual information can measure better similarity between images having different modalities i.e having different intensities at the same pixel positions. Gaussian curvature is a well known regularizer used for well posdness of a model, which preserve important structure in the process of registration of two images. The proposed model with Gaussian curvature works better for the large and smooth deformations without mesh folding while existing models with linear curvature may not produce better results for large deformations and may produce mesh folding. Thus we propose the following energy functional for registration of multi-modality images:

$$\min_{\mathbf{u}} \mathcal{J}(T, R; \mathbf{u}) = -\int_{\Omega} p^{T(\mathbf{u}),R}(t, s) \log \frac{p^{T(\mathbf{u}),R}(t, s)}{p^{T(\mathbf{u})}(t)p^{R}(s)} dtds + \alpha \sum_{m=1}^{2} \int_{\Omega} \left| \frac{u_{m,xy}u_{m,yx} - u_{m,xx}u_{m,yy}}{(u_{m,x}^2 + u_{m,y}^2 + 1)^2} \right| d\Omega, \tag{12}$$

where $\alpha > 0$ is a trade off parameter. Minimization of the proposed model in (12) with respect to u_m for $m = 1, 2$ leads to the following Euler Lagrange equations:

$$\begin{cases} \alpha\nabla \cdot \left(\dfrac{4 \mid u_{1,xy}u_{1,yx} - u_{1,xx}u_{1,yy} \mid}{\mathcal{M}_1^3} \nabla u_1 \right) + \alpha\nabla \cdot \mathcal{C}_{1,1} \\ \quad + \alpha\nabla \cdot \mathcal{C}_{1,2} + F_1 = 0, \\ \alpha\nabla \cdot \left(\dfrac{4 \mid u_{2,xy}u_{2,yx} - u_{2,xx}u_{2,yy} \mid}{\mathcal{M}_2^3} \nabla u_2 \right) + \alpha\nabla \cdot \mathcal{C}_{2,1} \\ \quad + \alpha\nabla \cdot \mathcal{C}_{2,2} + F_2 = 0, \end{cases} \tag{13}$$

where

$$\mathcal{M}_m = u_{m,x}^2 + u_{m,y}^2 + 1,$$
$$\mathcal{C}_{m,1} = \left(\left(-\frac{\mathcal{S}_m u_{m,yy}}{\mathcal{M}_m^2} \right)_x, \left(\frac{\mathcal{S}_m u_{m,xy}}{\mathcal{M}_m^2} \right)_x \right),$$
$$\mathcal{C}_{m,2} = \left(\left(\frac{\mathcal{S}_m u_{m,yx}}{\mathcal{M}_m^2} \right)_y, \left(-\frac{\mathcal{S}_m u_{m,xx}}{\mathcal{M}_m^2} \right)_y \right),$$
$$\mathcal{S}_m = sign(u_{m,xy}u_{m,yx} - u_{m,xx}u_{m,yy}), \quad m = 1, 2.$$

The Gâteaux derivative of the mutual information distance measure [36] is given as

$$F = (F_1, F_2)^t = \frac{1}{|\Omega|} \left[\mathcal{K} * \frac{\partial E(R, T(\mathbf{u}))}{\partial t} \right] \nabla_u T(\mathbf{u})),$$

it implies that

$$\frac{\partial E(R, T(\mathbf{u}))}{\partial t} = \frac{1}{p^{R,T(\mathbf{u}))}(s, t)} \frac{\partial p^{R,T(\mathbf{u}))}(s, t)}{\partial t} - \frac{1}{p^{T(\mathbf{u}))}(t)} \frac{\partial p^{T(\mathbf{u})}(t)}{\partial t},$$

and

$$E = 1 + \log \frac{p^{T(\mathbf{u}),R}(t, s)}{p^{R}(s)p^{T(\mathbf{u})}(t)}$$

where $|\Omega|$ denotes the area of the image domain and $\mathcal{K}$ is the smooth density kernel used to estimate the joint probability density function of images $T(\mathbf{u})$ and R given by $p^{T(\mathbf{u}),R}(t, s)$. $*$ denotes the convolution operator. The boundary conditions are:

$$\left(\frac{\mathcal{S}_m(u_{m,y})_y}{\mathcal{M}_m^2}, \frac{\mathcal{S}_m(u_{m,y})_x}{\mathcal{M}_m^2} \right) \cdot \hat{n} = 0,$$
$$\left(\frac{\mathcal{S}_m(u_{m,x})_y}{\mathcal{M}_m^2}, \frac{\mathcal{S}_m(u_{m,x})_x}{\mathcal{M}_m^2} \right) \cdot \hat{n} = 0,$$

for $m = 1, 2$ and $\hat{n}$ denotes the normal vector at the boundary $\partial\Omega$. The Augmented Lagrangian method (ALM) is used to solve the proposed model, where the detailed explanation is given in section III.

Energy Functional 2*:* The energy functional for our second proposed model is based on normalized gradient field (NGF) as similarity measure combined with the Gaussian curvature as regularizer work better for large and smooth deformations without mesh folding. Normalized gradient field can align the edges of different structures in the reference and the transformed template images. The basic idea of the normalized gradient field is to use image gradient norm. Through the gradients of the reference and template images the features can be identified by the intensity changes. The energy functional is given as;

$$\min_{\mathbf{u}} \mathcal{J}(T, R; \mathbf{u}) = \int_{\Omega} \left(1 - \left((nT(\mathbf{u}))^t \cdot nR \right)^2 \right) d\Omega + \alpha \sum_{m=1}^{2} \int_{\Omega} \left| \frac{u_{m,xy}u_{m,yx} - u_{m,xx}u_{m,yy}}{(u_{m,x}^2 + u_{m,y}^2 + 1)^2} \right| d\Omega, \tag{14}$$

where α is the positive trade off parameter. Minimizing this functional with respect u_1, u_2 leads to the following

Euler Lagrange equations:

$$\begin{cases} \alpha\nabla\cdot\Big(\dfrac{4\mid u_{1,xy}u_{1,yx}-u_{1,xx}u_{1,yy}\mid}{\mathcal{M}_1^3}\nabla u_1\Big)+\alpha\nabla\cdot\mathcal{C}_{1,1} \\ \qquad +\alpha\nabla\cdot\mathcal{C}_{1,2}+F_1=0, \\ \alpha\nabla\cdot\Big(\dfrac{4\mid u_{2,xy}u_{2,yx}-u_{2,xx}u_{2,yy}\mid}{\mathcal{M}_2^3}\nabla u_2\Big)+\alpha\nabla\cdot\mathcal{C}_{2,1} \\ \qquad +\alpha\nabla\cdot\mathcal{C}_{2,2}+F_2=0, \end{cases} \tag{15}$$

where

$$\begin{aligned} \mathcal{M}_m &= u_{m,x}^2+u_{m,y}^2+1, \\ \mathcal{C}_{m,1} &= \Big(\Big(-\frac{\mathcal{S}_m u_{m,yy}}{\mathcal{M}_m^2}\Big)_x,\Big(\frac{\mathcal{S}_m u_{m,xy}}{\mathcal{M}_m^2}\Big)_x\Big), \\ \mathcal{C}_{m,2} &= \Big(\Big(\frac{\mathcal{S}_m u_{m,yx}}{\mathcal{M}_m^2}\Big)_y,\Big(-\frac{\mathcal{S}_m u_{m,xx}}{\mathcal{M}_m^2}\Big)_y\Big), \\ \mathcal{S}_m &= sign(u_{m,xy}u_{m,yx}-u_{m,xx}u_{m,yy}), \qquad m=1,2, \end{aligned}$$

and

$$F=(F_1,F_2)^t=\frac{2(nT(\mathbf{u})^t nR)H(T(\mathbf{u}))}{||nT(\mathbf{u})||_\epsilon}[nR-(nT(\mathbf{u})^t nR)nT(\mathbf{u})],$$

where $H_{ij}(T(\mathbf{u}))$ is the Hessian matrix of $T(\mathbf{u})$ for $i,j=1,2$.

The boundary conditions are:

$$\begin{aligned} \Big(\frac{\mathcal{S}_m(u_{m,y})_y}{\mathcal{M}_m^2},\frac{\mathcal{S}_m(u_{m,y})_x}{\mathcal{M}_m^2}\Big)\cdot\hat{n}=0, \\ \Big(\frac{\mathcal{S}_m(u_{m,x})_y}{\mathcal{M}_m^2},\frac{\mathcal{S}_m(u_{m,x})_x}{\mathcal{M}_m^2}\Big)\cdot\hat{n}=0, \end{aligned}$$

for $m=1,2$ and $\hat{n}$ denotes the normal vector at the boundary $\partial\Omega$. This model can also be solved by Augmented Lagrangian method. Here, we discuss the discretization of MI and NGF [15], [41].

1) DISCRETIZATION OF MUTUAL INFORMATION

The two images T and R are assumed within the range $[t_0, t_m]$ and $[s_0, s_m]$ respectively, where $t_0=s_0=0$ and $t_m=s_m=255$. Here h_t and h_s are defined as $h_t=\frac{t_m-t_0}{m_t}$ and $h_s=\frac{s_m-s_0}{m_s}$, where m_t and m_s are pre-defined bin numbers and we need to discretize the intensity values of T and R. We have $t_i=t_0+(i-0.5)h_t$ and $s_j=s_0+(j-0.5)h_s$, $i=0,\ldots,m_t$, $j=0,\ldots,m_s$.

I_T and I_R be the discrete set of intensity values in T and R respectively. The joint discrete Parzen Window histogram is defined as

$$h(t,s)=\frac{1}{m_t m_s}\sum_{x\in\Omega^\upsilon}^{N} g_k{}^{\sigma T}(t-t_i(x))g_k{}^{\sigma R}(s-s_j(x)), \tag{16}$$

and the joint probability distribution is defined as

$$p(t,s)=p^{T,R}(t,s)=\frac{1}{\sum_{t\in I_T}\sum_{s\in I_R}h(t,s)}h(t,s), \tag{17}$$

A small tolerance ϵ is added to the argument of the logarithm to deal with the case $0log0$. The joint entropy of images T and R can be written as

$$H(T,R)=m_t m_s\sum_{i=1}^{m_t}\sum_{j=1}^{m_s}p_{i,j}log(p_{i,j}+\epsilon), \tag{18}$$

where $p_{i,j}=p(t_i,s_j)$. The marginal densities and the entropies are given as

$$\begin{aligned} p^T(t_k)&=m_s\sum_{j=1}^{m_s}p_{k,j}, \quad H(T)=m_t\sum_{k=1}^{m_t}p^T(t_k)log(p^T(t_k)+\epsilon), \\ p^R(s_k)&=m_t\sum_{i=1}^{m_t}p_{i,k}, \quad H(R)=m_s\sum_{k=1}^{m_s}p^R(s_k)log(p^R(s_k)+\epsilon), \end{aligned} \tag{19}$$

for the computation of MI.

2) DISCRETIZATION OF NGF

The distance measure NGF is basically an $\mathcal{L}_2$-norm of residual r, where the residual measures the alignment of the normalized gradients in two images at a pixel position $\mathbf{x}$,

$$r^h(\mathbf{x})=1-\Big(\Big(nT(\mathbf{x})\Big)^t nR(\mathbf{x})\Big)^2, \tag{20}$$

by using finite difference method for discrete images R and T of size $M\times M$. Both images are discretized using cell centered discretization on a uniform grid where $\mathbf{x}_{j,i}$ shows the pixel position. A non-uniform grid can also be used with finite difference method. The gradient can be calculated by using

$$\begin{aligned} \partial_x T^h(\mathbf{x}_{j,i})&=\frac{T^h(x_{j+1,i})-T^h(x_{j-1,i})}{2h}, \\ \partial_y T^h(\mathbf{x}_{j,i})&=\frac{T^h(x_{j,i+1})-T^h(x_{j,i-1})}{2h}, \end{aligned} \tag{21}$$

where to approximate the first order derivatives, we use first order central differences. To reorder R and T into a row vector of size $M^2\times 1$ we use lexicographical ordering. Then we have the matrices of order $M^2\times M^2$

$$\mathcal{G}_x=\frac{1}{2h^2}\begin{bmatrix} -1 & 1 & 0 & \ldots & \ldots \\ -1 & 0 & 1 & 0 & \ldots \\ \vdots & \ddots & \ddots & \ddots & \vdots \\ \vdots & \ddots & -1 & 0 & 1 \\ \vdots & \ddots & 0 & -1 & 1 \end{bmatrix},$$

$$\mathcal{G}_y=\frac{1}{2h^2}\begin{bmatrix} -1 & -1 & 0 & \ldots & \ldots \\ 1 & 0 & -1 & 0 & \ldots \\ \vdots & \ddots & \ddots & \ddots & \vdots \\ \vdots & \ddots & 1 & 0 & -1 \\ \vdots & \ddots & 0 & 1 & 1 \end{bmatrix},$$

which shows the discrete gradient operators in x and y respectively. We can also calculate

$$\begin{aligned} \mathbb{E}_{T,j}&=\sqrt{(\mathcal{G}_x T^h)_j+(\mathcal{G}_y T^h)_j+\epsilon_T^2}, \\ \mathbb{E}_{R,j}&=\sqrt{(\mathcal{G}_x R^h)_j+(\mathcal{G}_y R^h)_j+\epsilon_R^2}, j=1,2,\ldots,M^2. \end{aligned} \tag{22}$$

where

$$r_j=\Big(\frac{(\mathcal{G}_x T^h)_j}{\mathbb{E}_{Tj}}\Big)\Big(\frac{(\mathcal{G}_x R^h)_j}{\mathbb{E}_{Rj}}\Big)+\Big(\frac{(\mathcal{G}_y T^h)_j}{\mathbb{E}_{Tj}}\Big)\Big(\frac{(\mathcal{G}_y R^h)_j}{\mathbb{E}_{Rj}}\Big) \tag{23}$$

and

$$\mathcal{D}^{ngf}(T^h, R^h) = h^2 \sum_{j=1}^{N^2} 1 - (r_j)^2. \tag{24}$$

III. NUMERICAL METHOD

In order to solve the Euler Lagrange equations given in (13) and (15) which are non-linear, we use a fast numerical Augmented Lagrangian method (ALM). In literature, the Augmented Lagrangian method is successfully used in image de-noising and image registration for mono-modality images [14], [42].

A. AUGMENTED LAGRANGIAN METHOD

Here, it will be shown that how to implement the Augmented Lagrangian Method (ALM) for both the Gaussian curvature based image registration models for multi-modality images. This important method has a property of solving constrained optimization problems using unconstrained problems. When the constraints are included in the objective functional this method become similar to the penalty method and the problem is solved by using the alternating minimization of every sub-problems. The additional terms arises in ALM known as lagrange multipliers, when the constraints are incorporated in the objective functional.

First, the model in (12) is solved by using Augmented Lagrangian method. Two new dual variables z_1 and z_2 are introduced where $z_1 = \nabla u_1(x)$ and $z_2 = \nabla u_2(x)$. As a result a system of second order PDEs are obtained which are more feasible to the effective solution. First, the problem is reformulated as the following constrained optimization problem for Gaussian curvature image registration for multi-modality images using MI as similarity measure,

$$\min_{u_1,u_2,z_1,z_2} \mathcal{J}(u_1, u_2, z_1, z_2) = \mathcal{D}(T, R; \mathbf{u}(\mathbf{x})) + \alpha\mathcal{S}^{(gc)}(z_1) + \alpha\mathcal{S}^{(gc)}(z_2), \tag{25}$$

such that $z_1 = \nabla u_1(x)$ and $z_2 = \nabla u_2(x)$ and further reformulate the above problem to obtain the Augmented Lagrangian functional

$$\begin{aligned}\mathcal{L}^{(gc)}&(u_1, u_2, z_1, z_2; \lambda_1, \lambda_2)\\ &= -\int_{\mathbb{R}^2} p^{T(\mathbf{u}),R}(t,s) \log \frac{p^{T(\mathbf{u}),R}(t,s)}{p^{T(\mathbf{u})}(t)p^R(s)} dtdr + \alpha\mathcal{S}^{(gc)}(z_1)\\ &\quad + \alpha\mathcal{S}^{(gc)}(z_2) + \langle\lambda_1, z_1 - \nabla u_1\rangle + \langle\lambda_2, z_2 - \nabla u_2\rangle\\ &\quad + \frac{r}{2}\|z_1 - \nabla u_1\|_2^2 + \frac{r}{2}\|z_2 - \nabla u_2\|_2^2,\end{aligned} \tag{26}$$

where λ_1, λ_2 are the Lagrange multipliers and r is a positive constant. To find the optimal values of the u_1, u_2, z_1, z_2 and λ_1, λ_2 an alternating minimization procedure is used and two main steps are involved in this process.

First Step: In this step we need to update z_1, z_2 for any given $u_1, u_2, \lambda_1, \lambda_2$. The objective functional can be written in the form

$$\begin{aligned}\min_{z_1,z_2} \alpha\mathcal{S}^{(gc)}(z_1) + \alpha\mathcal{S}^{(gc)}(z_2) + \langle\lambda_1, z_1\rangle + \langle\lambda_2, z_2\rangle\\ + \frac{r}{2}\|z_1 - \nabla u_1\|^2 + \frac{r}{2}\|z_2 - \nabla u_2\|^2.\end{aligned} \tag{27}$$

The following Euler Lagrange equations are used to solve this sub problem:

$$\begin{cases} -\alpha\Big(\Big(\frac{(-z_{1,1})_y}{\Gamma_1^2}\Big)_x + \Big(\frac{(-z_{1,1})_x}{\Gamma_1^2}\Big)_y\Big) - \alpha\frac{4S_1\mathbf{D}_1 z_{1,2}}{\Gamma_1^3}\\ \quad + \lambda_{1,2} + r(z_{1,2} - (u_1)_y) = 0\\ -\alpha\Big(\Big(\frac{(z_{1,2})_y}{\Gamma_1^2}\Big)_x + \Big(\frac{(-z_{1,2})_x}{\Gamma_1^2}\Big)_y\Big) - \alpha\frac{4S_1\mathbf{D}_1 z_{1,1}}{\Gamma_1^3} + \lambda_{1,2}\\ \quad + r(z_{1,1} - (u_1)_x) = 0, \end{cases} \tag{28}$$

where

$$\begin{aligned}\mathbf{D}_1 &= det(\nabla z_1) = (z_{1,1})_x(z_{1,2})_y - (z_{1,1})_y(z_{1,2})_x,\\ \Gamma_1 &= 1 + u_{1,x}^2 + u_{1,y}^2,\end{aligned}$$

and

$$S_1 = sign\Big(\frac{\mathbf{D}_1}{(\|\nabla u_1\|^2 + 1)^2}\Big).$$

If solving alternatively, there is a closed form solution for this first step, where

$$z_{1,1} = \frac{\Gamma_1^3\Big(-\alpha\Big(\Big(\frac{(z_{1,2})_y}{\Gamma_1^2}\Big)_x + \Big(\frac{(-z_{1,2})_y}{\Gamma_1^2}\Big)_y\Big)\Big) + \lambda_{1,1} + r(u_1)_x}{-r\Gamma_1^3 + \alpha 4S_1\mathbf{D}_1}.$$

$$z_{1,2} = \frac{\Gamma_1^3\Big(-\alpha\Big(\Big(\frac{(z_{1,1})_y}{\Gamma_1^2}\Big)_x + \Big(\frac{(-z_{1,1})_x}{\Gamma_1^2}\Big)_y\Big)\Big) + \lambda_{1,2} + r(u_1)_y}{-r\Gamma_1^3 + \alpha 4S_1\mathbf{D}_1}.$$

Similarly, we solve $z_{2,1}, z_{2,2}$ from the Euler lagrange equations:

$$\begin{cases} -\alpha\Big(\Big(\frac{(-z_{2,1})_y}{\Gamma_2^2}\Big)_x + \Big(\frac{(-z_{2,1})_x}{\Gamma_2^2}\Big)_y\Big) - \alpha\frac{4S_2\mathbf{D}_2 z_{2,2}}{\Gamma_2^3} + \lambda_{2,2}\\ \quad + r(z_{2,2} - (u_2)_y) = 0\\ -\alpha\Big(\Big(\frac{(z_{2,2})_y}{\Gamma_2^2}\Big)_x + \Big(\frac{(-z_{2,2})_x}{\Gamma_2^2}\Big)_y\Big) - \alpha\frac{4S_2\mathbf{D}_2 z_{2,1}}{\Gamma_2^3} + \lambda_{2,1}\\ \quad + r(z_{2,1} - (u_2)_x) = 0, \end{cases} \tag{29}$$

where

$$\begin{aligned}\mathbf{D}_2 &= det(\nabla z_2) = (z_{2,1})_x(z_{2,2})_y - (z_{2,1})_y(z_{2,2})_x,\\ \Gamma_2 &= 1 + u_{1,x}^2 + u_{1,y}^2,\end{aligned}$$

and

$$S_2 = sign\Big(\frac{\mathbf{D}_2}{(\|\nabla u_2\|^2 + 1)^2}\Big).$$

Second Step: Here we need to update u_1, u_2 for any given variables z_1, z_2 and λ_1, λ_2 with the new functional

$$\begin{aligned}\min_{u_1,u_2} -\int_{\mathbb{R}^2} p^{T(\mathbf{u}),R}(t,s) \log \frac{p^{T(\mathbf{u}),R}(t,s)}{p^{T(\mathbf{u})}(t)p^R(s)} dtdr - \langle\lambda_1, \nabla u_1\rangle\\ -\langle\lambda_2, \nabla u_2\rangle + \frac{r}{2}\|z_1 - \nabla u_1\|^2 + \frac{r}{2}\|z_2 - \nabla u_2\|^2.\end{aligned}$$

So the following Euler Lagrange equations are obtained,

$$\begin{cases} -r\Delta u_1 + F_1 + \nabla\cdot\lambda_1 + r\nabla\cdot z_1 = 0\\ -r\Delta u_2 + F_2 + \nabla\cdot\lambda_2 + r\nabla\cdot z_2 = 0 \end{cases} \tag{30}$$

with Neumann boundary conditions $\nabla u_m \cdot n = 0$, $m = 1, 2$. Before solving (30), we first linearize F using Taylor's expansion

$$\begin{aligned} F_m(u_1^{(n+1)}, u_2^{(n+1)}) &= F_m(u_1^{(n)}, u_2^{(n)}) + \partial_{u_1} F_m(u_1^{(n)}, u_2^{(n)})\delta u_1^{(n)} \\ &\quad + \partial_{u_2} F_m(u_1^{(n)}, u_2^{(n)})\delta u_2^{(n)} + \dots \\ &\approx F_m(u_1^{(n)}, u_2^{(n)}) + \sigma_{m,1}^{(n)}\delta u_1^{(n)} + \sigma_{m,2}^{(n)}\delta u_2^{(n)}, \end{aligned}$$

where

$$\begin{aligned} &\sigma_{m,1}^{(n)} = \partial_{u_1} F_m(u_1^{(n)}, u_2^{(n)}), \sigma_{m,2}^{(n)} = \partial_{u_2} F_m(u_1^{(n)}, u_2^{(n)}), \\ &\delta u_1^{(m)} = u_1^{(n+1)} - u_1^{(n)}, \delta u_2^{(m)} = u_2^{(n+1)} - u_2^{(n)}. \end{aligned}$$

Next, we approximate $\sigma_{m,1}^n$ and $\sigma_{m,2}^n$ by using

$$\sigma_{m,1}^{(n)} = \Big(\partial u_1\Big(\frac{1}{|\Omega|}\Big(\mathcal{K} * \frac{\partial E(R, T(x+\mathbf{u}^{(n)}))}{\partial t}\Big)\Big)\Big)\Big(\partial u_m T(x+\mathbf{u}^{(n)})\Big)$$

$$\sigma_{m,2}^{(n)} = \Big(\partial u_2\Big(\frac{1}{|\Omega|}\Big(\mathcal{K} * \frac{\partial E(R, T(x+\mathbf{u}^{(n)}))}{\partial t}\Big)\Big)\Big)\Big(\partial u_m T(x+\mathbf{u}^{(n)})\Big).$$

The discretization of (30) can be written as

$$\mathbf{A}^h(\mathbf{u}^{h,(n)})\mathbf{u}^{h,(n+1)} = \mathbf{B}^h(\mathbf{u}^{h,(n)}), \tag{31}$$

where

$$\mathbf{A}^h(\mathbf{u}^{(n)}) = \begin{bmatrix} -r\mathcal{L} + \sigma_{11}^h(\mathbf{u}^{h,(n)}) & \sigma_{12}^h(\mathbf{u}^{h,(n)}) \\ \sigma_{21}^h(\mathbf{u}^{h,(n)}) & -r\mathcal{L} + \sigma_{22}^h(\mathbf{u}^{h,(n)}) \end{bmatrix},$$

$$\mathbf{B}^h(\mathbf{u}^{(n)}) = \begin{bmatrix} -g_1^h + F_1^h(u_1^{(n)}, u_2^{(n)}) + \sigma_{11}^h(\mathbf{u}^{(n)})u_1^{h,(n)} + \\ \sigma_{12}^h(\mathbf{u}^{h,(n)})u_2^{h,(n)} \\ -g_2^h + F_2^h(u_1^{(n)}, u_2^{(n)}) + \sigma_{21}^h(\mathbf{u}^{(n)})u_1^{h,(n)} + \\ \sigma_{22}^h(\mathbf{u}^{h,(n)})u_2^{h,(n)} \end{bmatrix}.$$

where $\mathcal{L}$ is the discrete version of Laplace operator Δ and g_m^h is the discrete version of

$$\nabla \cdot \lambda_m + r\nabla \cdot z_m, \quad m = 1, 2.$$

In the last, the system of equations is solved in (31) by using weighted point wise Gauss Siedel method

$$\mathbf{u}^{h,(n+1)} = (1-\omega)\mathbf{u}^{h,(n)} + \omega(\mathbf{A}^h(\mathbf{u}^{(n)}))^{-1}\mathbf{B}^h(\mathbf{u}^{(n)}),$$

where $\omega \in (0, 1)$ and we take $\omega = 0.9725$.

Similarly, we can reformulate the problem for model 2 by replacing NGF as similarity measure.

Various steps of the proposed models are shown in block diagram in Fig. 1.

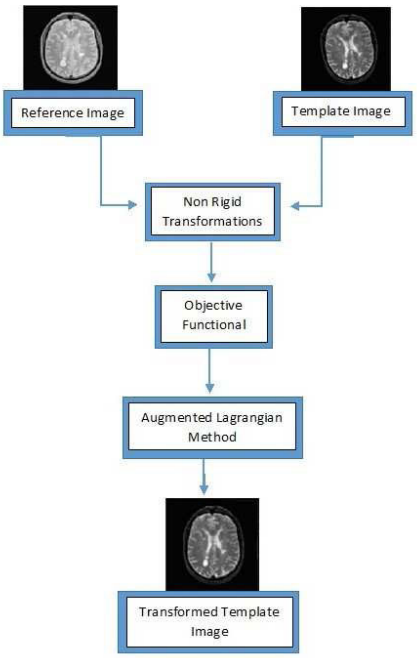

FIGURE 1. Block diagram of the proposed models.

IV. EXPERIMENTAL RESULTS

In this section, the performance of the proposed models is assessed by using numerical experiments to examine the robustness and efficiency of the algorithm for multi-modality images. The minimum value of the determinant of the jacobian matrix J of the transformation is calculated, to judge the quality of the alignment of the images and to observe the folding and cracking of the deformed grid. The value is denoted by $\mathcal{E}$

$$J = \begin{bmatrix} 1 + u_{1,x} & u_{1,y} \\ u_{2,x} & 1 + u_{2,y} \end{bmatrix}, \quad \mathcal{E} = min(det(J)),$$

where $u_{1,x}$ and $u_{1,y}$ denotes the gradient of u_1 whereas $u_{2,x}$ and $u_{2,y}$ denotes the gradient of u_2. Experimentally, we observed that $r = 0.001$ and 0.01 works well for several types of images. As for stoping criteria $tol = 0.001$ is used. Experiments were carried out by Matlab2015a with Intel core i7, 7th generation and INTEL Xeon 2640 with cores 40, RAM 128GB.

A. TEST 1: TEST ON PAIR OF PHOTON DENSITY (PD) WEIGHTED MRI AND T2-MRI

Medical images for this test are taken from [28] where the reference image is from photon density weighted MRI and the template image represents T2-MRI. Both of the images are of the size 128×128. The results of the proposed Gaussian curvature model 1 in (12) using MI as similarity measure for this test are shown in Fig.2. It Can be observed that the proposed model 1 in (12) is able to register real medical images very accurately. We show the results of the proposed model 2 in (14) using NGF as similarity measure for this test in Fig. 3. In both the models (12) and (14), different regularization parameters are tested. Here the optimal choices of parameters are considered as $\alpha = 8$ for model in (12) and $\alpha = 5$ for model in (14) respectively. These parameters are chosen as optimal choices such as the transformed template images are very similar to the reference images and also the transformations do not suffer from mesh folding. For Gaussian curvature model 2 in (14) using NGF as similarity measure there is essentially one parameter to tune i.e. the edge parameter (η). In our experiments η ranges in [3:10]. For the proposed model 2 in (14), the transformed template image is shown in Fig. 3 (b). We can see that the transformed template

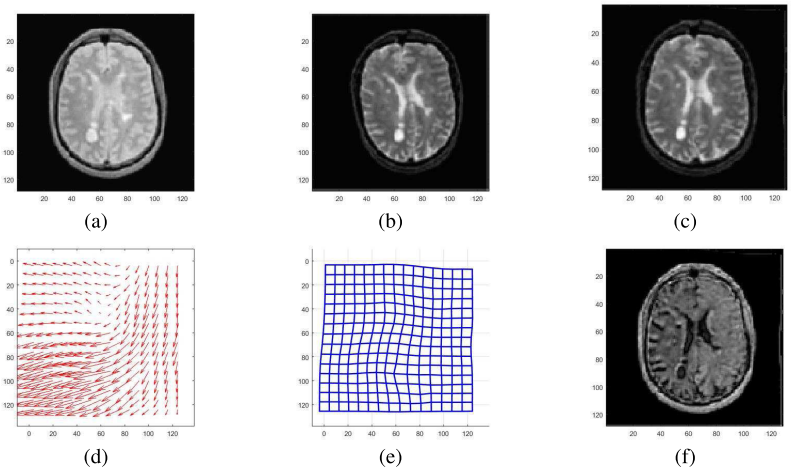

FIGURE 2. The results of the proposed Gaussian curvature model 1 in (12) using MI as similarity measure for multi-modality image registration. The initial reference image R, the template image T with with $MI(T, R) = -0.51393$, the transformed template image $T(\mathbf{u})$ with $\text{MI}(T(\mathbf{u}), R) = -0.88925$, the displacement field, the transformations and the differences between the transformed template image and reference image are shown in (a-f) respectively. Here the value of $\mathcal{E} = -1.8653 < 0$. From (c) we can see that the proposed Gaussian Curvature model 1 in (12) using MI as similarity measure indicates a good alignment between the transformed template image $T(\mathbf{u})$ in (c) and the reference image R in (a). The transformed template image in (c) appears to be very similar to the reference image in (a).

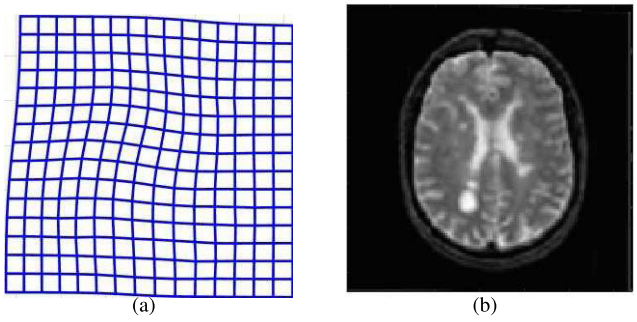

FIGURE 3. The results of the proposed Gaussian curvature model 2 in (14) using NGF as similarity measure for multi modality images. The resulting transformed template image in (b) with $MI(T(u), R) = -0.9296$ is perfectly aligned with the reference image. The smaller value of $MI(T(\mathbf{u}), R) = -0.9296$ in (b) than in Fig. 2 (c) i.e. $\text{MI}(T(\mathbf{u}), R) = -0.88925$, shows a higher similarity between the transformed template and the reference images.

in Fig. 3 (b) and the reference images in Fig. 2 (a) have an acceptable level of alignment and give quite satisfactory results. From the experimental tests we can observed that for this test both the proposed models in (12) and (14) performs very well.

For this test by Gaussian curvature model 1 in (12) using MI as similarity measure, we need $k = 6$ outer iterations and $\mathcal{E} < 0$ for better alignment of the transformed template image and reference image as shown in Fig. 2. In Fig. 3 (a) the transformation graph can be observed for the proposed model 2 in (14) and Fig. 3 (b) shows the registered image using the proposed model in (14). Here we need two outer iterations to get the value $MI(T(\mathbf{u}), R) = -0.9296$ in Fig. 3 (b) which is smaller than the value of $MI(T(\mathbf{u}), R) = -0.88925$ in Fig. 2 (c) which indicates higher similarity between the reference and the transformed template images. For solving the proposed models, we use the Augmented Lagrangian Method which has four dual variables and four Lagrange multipliers terms therefore they requires more computational time. In Fig. 4 (a) and (b) shows the effect on the values of $\mathcal{E}$ for various values of k and α, where $\mathcal{E} < 0$ for better registration results. We obtain this figure using $r = 0.01$ for this test and it confirms that α controls the smoothness of the deformation field. In Fig. 4 (c) the energy vs. iterations graph is shown. Since the energy functional is increasing, which confirms the convergence of the proposed model in (12).

B. TEST 2: TEST ON SYNTHETIC IMAGES

In this test, our aim is to investigate capabilities of both the proposed Gaussian curvature models in (12) and (14) for registration of synthetic images of size 128×128. Here, we illustrate the type of images where the proposed GC model 2 using NGF as similarity measure delivers good registration results than GC model 1 using MI as similarity measure. Here, the template image is chosen as a synthetic noisy image with Gaussian noise. From Fig. 5 it can be observed that the result of the GC model 1 using MI as similarity measure in (12) for multi modality images fails to deform the inner part of the image. Here, the GC model having MI as similarity measure is tested for different values of regularization parameter and the optimal choice of the parameter $\alpha = 9$ is considered. Also, from Fig. 5 we can see that for $k = 3$ the value of $MI = -0.51882$ and the value of $\mathcal{E} = -0.012703 < 0$ is decreasing which indicates the similarity between the transformed template image and reference image except the middle part of the image.

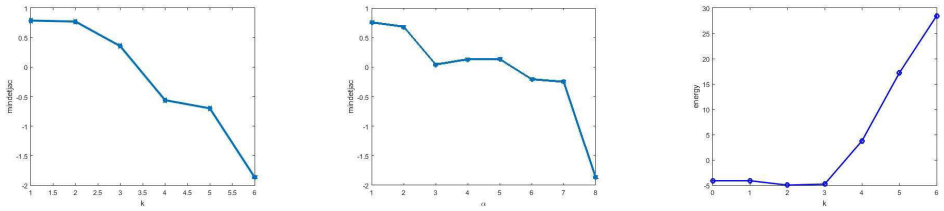

FIGURE 4. The iterations (k) and mindetjac ($\mathcal{E}$) history is shown in (a). The effect of values of mindetjac ($\mathcal{E}$) and α are shown in (b) and the energy graph is shown in (c).

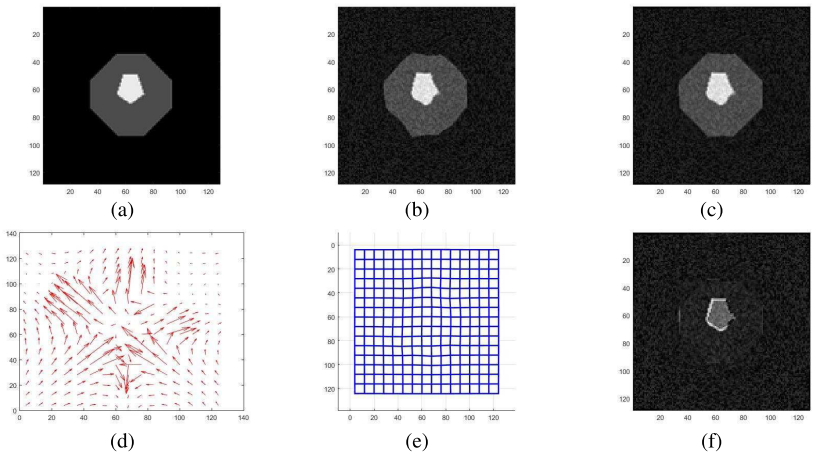

FIGURE 5. The results of the proposed Gaussian curvature model 1 in (12) using MI as similarity measure for multi-modality image registration. The initial reference image R, the template image T with $MI(T, R) = -0.48668$, the transformed template image $T(\mathbf{u})$ with $\text{MI}(T(\mathbf{u}), R) = -0.51882$, the displacement field, the transformations and the differences between the transformed template image and reference image are shown in (a-f) respectively. Here the value of $\mathcal{E} = -0.012703 < 0$. We can see that the transformed template image is similar to the reference image except the inner white part of the image.

In Fig. 6 the result for the proposed Gaussian curvature model 2 is shown in (14) using NGF as similarity measure. The resulting transformed template image for the normalized gradient field is indicated in Fig. 6 (b) which shows a good alignment with the reference image in Fig. 5 (a). Here, an acceptable level of transformed template image is obtained where it appears to be similar to the reference image. Smaller value of $MI(T(\mathbf{u}), R) = -0.5504$ in Fig. 6 (b) than in Fig. 5 (c) indicates higher similarity between the reference and transformed template images. From this test, it can be figured out that the Gaussian curvature model 2 in (14) using NGF as similarity measure out performs the Gaussian curvature model 1 in (12) using MI as similarity measure, in the registration of noisy images.

In Fig. 7(a) the mindetjac vs. iterations is displayed where for $k = 3$ the value of mindetjac < 0 and $r = 0.01$. The effect on the values of $\mathcal{E} < 0$ for various values of α are shown in Fig. 7(b), which confirms that α controls the smoothness of the deformation field. The energy vs. iterations of ALM to the final solution is shown in Fig. 7(c). Based on this experiment from the energy graph in Fig. 7 (c), we can see that there should be 3 maximum outer iterations as $r = 0.01$.

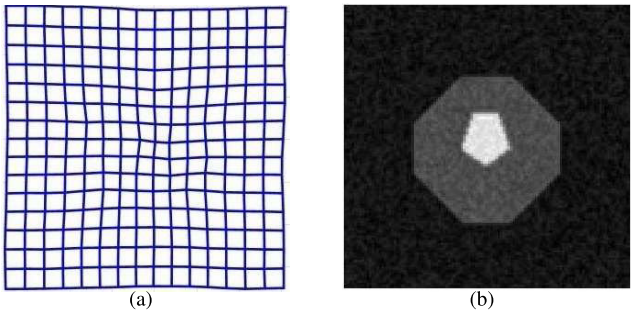

FIGURE 6. Results of the proposed Gaussian curvature model 2 in (14) using NGF as similarity measure for multi modality images. The resulting transformed template image in (b) with $MI(T(u), R) = -0.5504$ is perfectly aligned with the reference image. Smaller value of $MI(T(u), R) = -0.5504$ in (b) than in Fig. (5) (c) i.e. $\text{MI}(T(\mathbf{u}), R) = -0.51882$ shows a higher similarity between the transformed image and the reference image.

C. TEST 3: TEST ON BIAS FIELD IMAGES

Bias field or intensity inhomogeneity (IIH) or intensity non-uniformity (INU) in magnetic resonance imaging (MRI) is an artifact that is mainly produced by improper image acquisition process. It affects the intensities of the homogeneous tissue regions (for example, gray matter (GM), white

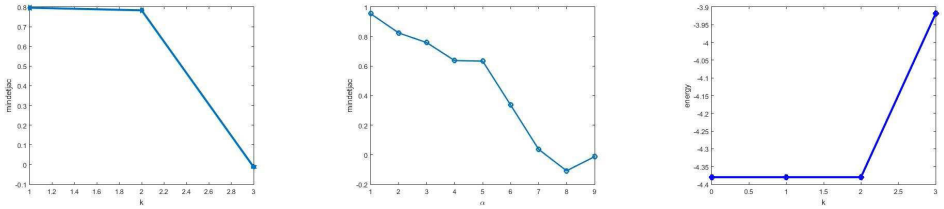

FIGURE 7. The effect of values of mindetjac ($\mathcal{E}$) vs. iterations and α vs. mindetjac ($\mathcal{E}$) are shown in (a)-(b). The energy vs. iteration graph is shown in (c).

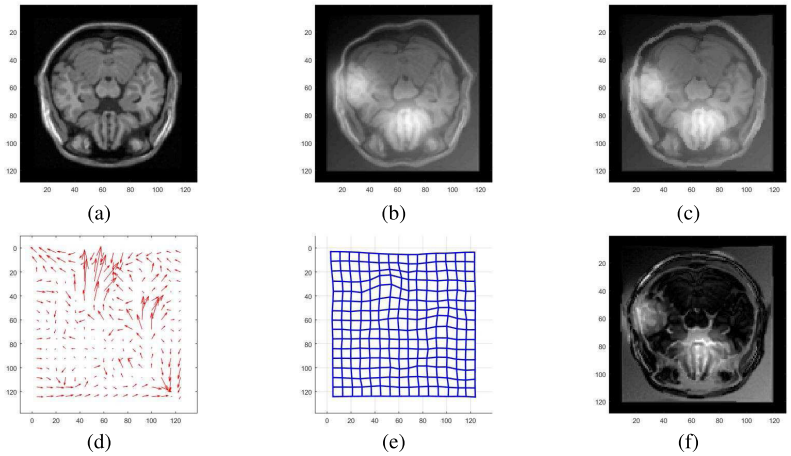

FIGURE 8. The results of the Gaussian curvature model 1 in (12) using MI as similarity measure for multi-modality image registration. The initial reference image R, the template image T with $MI(T, R) = -0.57587$, the transformed template image $T(\mathbf{u})$ with $\text{MI}(T(\mathbf{u}), R) = -0.77705$, the displacement field, the transformations and the differences between the transformed template and reference images are shown in (a-f) respectively. Here the value of $\mathcal{E} = -0.13075 < 0$. We can observe that due to strong bias field in (b) the model is unable to register the template image with the reference image.

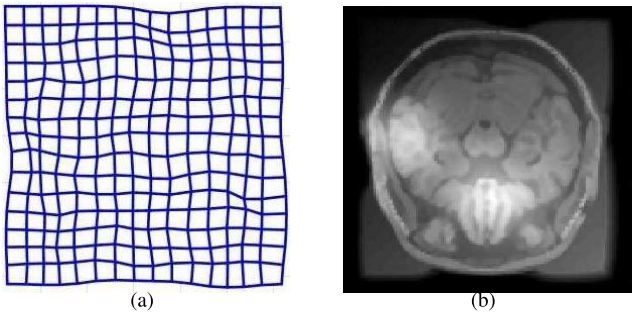

FIGURE 9. Results of the Gaussian curvature model 2 in (14) using NGF as similarity measure for multi modality images. The less value of $MI(T(\mathbf{u}), R) = -0.7787$ in (b) than in Fig.(8) (c) shows high similarity between the transformed template and reference images. The outer part of the transformed template image in Fig.(9) (c), having strong bias field has a good aligned with the reference image in Fig.8(a).

matter (WM) and cerebrospinal fluid (CSF) in MRI brain images). In bias field images some part of the same object appears to become darker than the rest of the object. We have run the experiments for brain MR images having strong bias field. For this test the images from [43] are considered where both the images are of size 128×128. It can be observed that for the proposed model 1 in (12) using MI as similarity measure the deformed grid is ruined for the third iteration i.e. at $k = 3$. The best result we have found for the problem is to fix $r = 0.001$ and varies α when $\alpha = 15$ and $k = 2$.

Based on these experiments it is found out that when $k = 1$ the values of $\mathcal{E} = 0.36602$ and $MI = -0.75984$. Next we need to observe that how to stop the iteration before the deformed grid is ruined. For this, the value of $\mathcal{E}$ after 2nd iteration which is $\mathcal{E} = -0.13075 < 0$. So the Gaussian curvature model 1 in (12) using MI works well for $\mathcal{E} < 0$. Also, we have figured out that the value of $MI = -0.77705$ in the 2nd iteration is decreasing, which indicates the higher similarity between the reference and transformed template image having strong bias field.

From the energy graph in Fig. 10(a) it can be analyzed that there should be 2 maximum iterations because for the third iteration the deformed grid is ruined therefore, we stop at $k = 2$. Here, the value of $r = 0.001$ is fixed.

D. TEST 4: TEST ON DATABASE

Brainweb [44] is a simulated brain database (SBD) contains a set of realistic MRI data volumes produced by an MRI simulator. The SBD contains simulated brain MRI data based on two anatomical models: normal and multiple

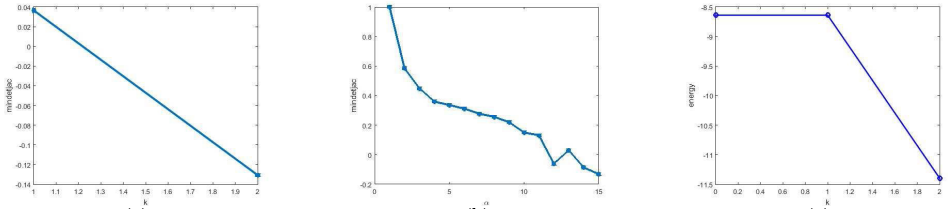

FIGURE 10. The iterations vs. mindetjac ($\mathcal{E}$) graph is shown in (a). The effect of values of mindetjac ($\mathcal{E}$) and α are shown in (b) and the energy graph is shown in (c).

TABLE 1. Gaussian Curvature model 1 using MI with best α.

Modality	Alpha (α)	Iteration No.	Mutual Information (MI) Values
T1-T2	10	1	-0.8049
		2	-0.81874
		3	-0.83072
		4	**-0.83896**
		5	-0.82154
		6	-0.69223
		7	-0.5523
		8	-0.25229
		9	-0.0154
		10	-0.01039
T1-PD	15	1	-0.93813
		2	**-0.95214**
		3	-0.92969
		4	-0.94361
		5	-0.44288
		6	-0.49434
		7	-0.50582
		8	-0.49211
		9	-0.51299
		10	-0.43469

sclerosis (MS) of 20 subjects. For both of these, full 3-dimensional data volumes have been simulated using three sequences (T1, T2, and photon-density (PD) weighted) MRI and a variety of slice thicknesses, noise levels, and levels of intensity non-uniformity. In this test the implementation of the proposed models in (12) and (14) having MI and NGF as similarity measures are demonstrated on normal brain MRI images taken from Brainweb. Here two pairs of MRI brain images of randomly selected subject 04 from 20 available subjects of normal brain are used. We have taken MRI sequence T1 as template image and normal phantom with MRI sequence T2 and PD as reference images. The resolution of reference and template images are $181 \times 217 \times 181$ and $256 \times 256 \times 181$ respectively. The central slice (slice no. 91) from both reference and template images is considered and is re-sized to same scale of 128×128 resolution. T1 is taken as template image for both cases of reference images (T2 and PD). Here, we have fixed the value of $r = 0.01$. The Table 1 shows the Gaussian Curvature model 1 in (12) using MI as similarity measure with best α and Table 2 shows the Gaussian Curvature model 2 in (14) using NGF with best α and edge parameter η.

Fig. 11 shows the graph of Gaussian Curvature model 1 in (12) using MI as similarity measure for data set T1-T2 images. In Fig. 11 (a), (b), (c), the minimum values of MI are -0.7928 at iteration 3 and $\alpha = 5$, -0.839 at iteration 4 and $\alpha = 10$ and -0.834 at iteration 5 and $\alpha = 13$, for α ranges $[1 : 5]$, $[6 : 10]$ and $[11 : 15]$ respectively. The overall minimum MI value for α range $[1 : 15]$ is -0.839 at iteration 4 and $\alpha = 10$.

Fig. 12 shows the graph of Gaussian Curvature model 1 in (12) using MI as similarity measure for data set T1-PD images. In Fig. 12(a), (b), (c), the minimum values of MI are -0.8635 at iteration 2 and $\alpha = 5$, -0.9177 at iteration 2 and $\alpha = 10$ and -0.95214 at iteration 2 and $\alpha = 15$, for α ranges $[1 : 5]$, $[6 : 10]$ and $[11 : 15]$ respectively. The overall minimum MI value for α range $[1 : 15]$ is -0.95214 at iteration 2 and $\alpha = 15$.

Fig. 13 shows the graph of Gaussian curvature model 2 in (14) using NGF as similarity measure for data set

TABLE 2. Gaussian Curvature model 2 using NGF with best Edge (η) and Alpha (α).

Modality	Edge (η)	Alpha (α)	Ite No.	Normalized Gradient Field (NGF) values
T1-T2	3	6	1	15.3297
			2	**15.2287**
			3	16.489
			4	17.457
			5	17.8249
			6	17.0567
			7	16.2942
			8	17.5759
			9	17.3074
			10	18.2164
T1-PD	5	11	1	2.9159
			2	**2.7775**
			3	4.018
			4	4.2373
			5	4.1357
			6	4.1307
			7	4.2641
			8	4.3984
			9	3.9613
			10	3.9796

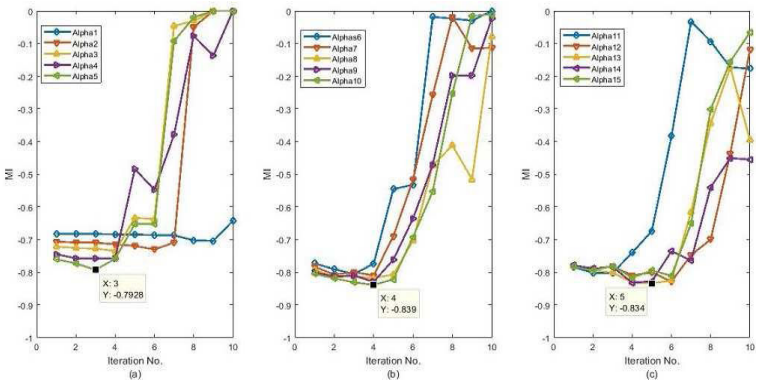

FIGURE 11. Gaussian Curvature model 1 using MI as similarity measure graph for T1-T2.

T1-T2 images. In Fig. 13 (a), (b), (c), the minimum values of *NGF* are 15.27 at iteration 2 and $\alpha = 3$, 15.23 at iteration 2, $\eta = 3$ and $\alpha = 6$ and 17.14 at iteration 10 and $\alpha = 12$, for α ranges $[1 : 5], [6 : 10]$ and $[11 : 15]$ respectively. The overall minimum *NGF* value for α range $[1 : 15]$ is 15.23 at iteration 2, $\alpha = 6$ and $\eta = 3$.

Fig. 14 shows the graph of Gaussian Curvature model 2 in (14) using NGF as similarity measure for data set T1-PD images. In Fig. 14 (a), (b), (c), the minimum values of NGF are 3.5462 at iteration 2 and $\alpha = 5$, 2.842 at iteration 2 and $\alpha = 10$ and 2.777 at iteration 2 and $\alpha = 11$, for α ranges $[1 : 5], [6 : 10]$ and $[11 : 15]$ respectively. We have analyzed our Gaussian curvature model using *NGF* as similarity measure, for edge ranges $[3 : 10]$ and found that $\eta = 3$ gives best results. The overall minimum NGF value for α ranges $[1 : 15]$ with $\eta = 5$ is 2.777 at iteration 2 and $\alpha = 11$.

From Table 3 it can be observed that Gaussian Curvature model 1 in (12) using MI for T1-T2 for best value of $\alpha = 10$ and at $k = 4$ iteration the value of $MI = -0.83896$ and Gaussian Curvature model 2 in (14) using NGF for T1-T2 for best value of $\alpha = 6$ and at $k = 2$ iteration the value of MI $= -0.84566$. Fig. 15 shows that the value of MI $= -0.84566$ for Gaussian curvature model 2 is less than the value of MI $= -0.83896$ for Gaussian curvature model 1 for T1-T2 images, which shows a higher similarity between the template image T1 and reference image T2. Here, the value of the mindetjac $(\mathcal{E}) < 0$. Also from Fig.16, for Gaussian Curvature model in (14) using NGF for T1-PD for the best value of $\alpha = 11$ at $k = 2$ iterations, the value

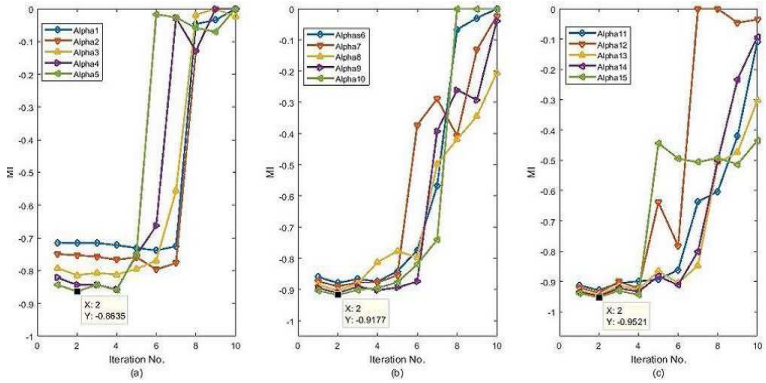

FIGURE 12. Gaussian Curvature model 1 using MI as similarity measure for T1-PD.

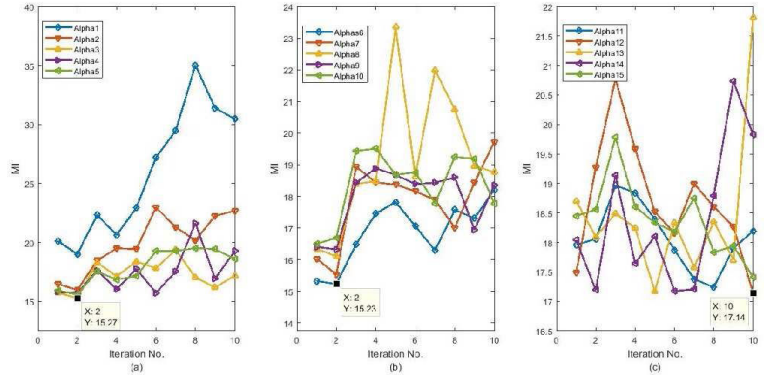

FIGURE 13. Gaussian Curvature model 2 using NGF as similarity measure for T1-T2.

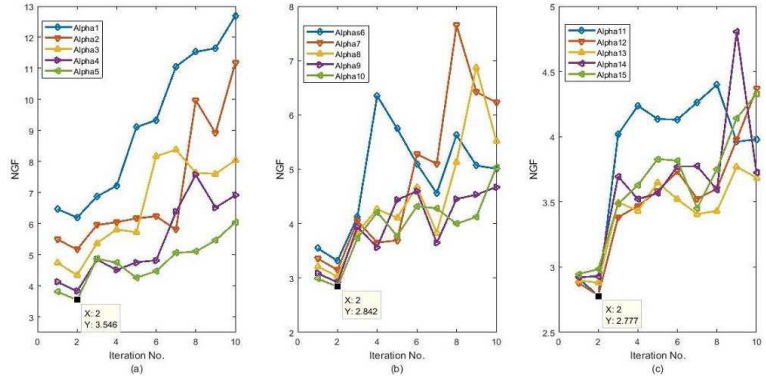

FIGURE 14. Gaussian Curvature model 2 using NGF as similarity measure for T1-PD.

TABLE 3. Comparison of the proposed Gaussian Curvature models using MI and NGF as similarity measures.

Modality	Models	Alpha	Iteration No	MI
T1-T2	Gaussian Curvature model 1 using MI	10	4	-0.83896
	Gaussian Curvature model 2 using NGF with best Edge=3	6	2	-0.84566
T1-PD	Gaussian Curvature model 1 using MI	15	2	-0.95214
	Gaussian Curvature model 2 using NGF with best Edge=5	11	2	-0.95244

of MI $= -0.95244$ which is less than the value of MI $= -0.95214$ for Gaussian Curvature model in (12) using MI for $\alpha = 15$ and $k = 2$ with the value of mindetjac $(\mathcal{E}) < 0$. Which indicates a good registration result between

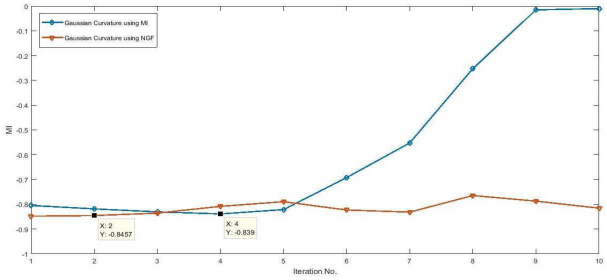

FIGURE 15. Comparison graph for T1-T2 of the proposed Gaussian Curvature models using MI and NGF as similarity measures.

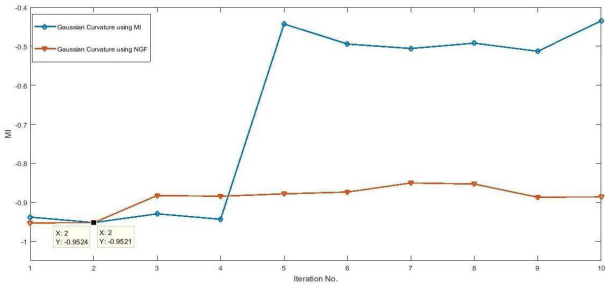

FIGURE 16. Comparison graph for T1-PD of the proposed Gaussian Curvature models using MI and NGF as similarity measures.

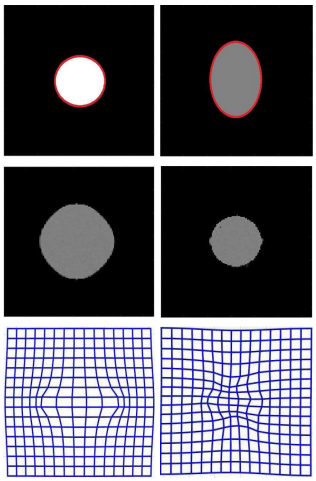

FIGURE 17. Comparison of the Gaussian curvature model 1 in (12) using MI as similarity measure and Gaussian curvature model 2 in (14) using NGF as similarity measure for multi-modality images. From Left: The initial reference image R (A white circle), the Template image T (A gray ellipse), the transformed template image of Gaussian curvature model 1 in (12) using MI as similarity measure with $JSC = 0.41333$ and the transformed template image of the Gaussian curvature model 2 in (14) using NGF as similarity measure with $JSC = 0.8591$, respectively. Clearly the Gaussian curvature model 2 using NGF as similarity measure works well while the Gaussian curvature model 1 using MI as similarity measure fails to register.

the template image T1 and reference image PD. From Fig. 15 and Fig. 16 we can see that the overall performance of the Gaussian curvature model 2 in (14) using NGF as similarity measure is better than the Gaussian curvature model 1 in (12) using MI as similarity measure.

E. TEST 5: JACCARD SIMILARITY COEFFICIENT (JSC)

The value of JSC lies between 0 (no over lapping) and 1 (perfect alignment). The value closer to 1 shows that the transformed template image is very similar to the reference image and the value closer to 0 indicates a lower similarity. In this example, a synthetic image from [30] is considered to illustrate the type of images where a good result for normalized gradient field than mutual information is obtained. Fig.17 shows the comparison of the proposed Gaussian curvature models in (12) and (14) using MI and NGF as similarity measures, respectively. Here, the Gaussian curvature models using mutual information (MI) and normalized gradient field (NGF) are tested for different regularization parameters. The optimal choices for the parameters are considered by making different tests, where we set $\alpha = 2$, $r = 0.01$, $\beta = 1$ and the iterations $k = 5$ for Gaussian curvature model 1 in (12) and $\alpha = 6$, $r = 0.01$, $\beta = 1$ and the iterations $k = 6$ for Gaussian curvature model 2 in (14). These optimal parameters are chosen such that the transformed template image is very similar to the reference image and the transformations do not suffer with mesh folding. For quantitative comparison, the Jaccard similarity coefficient (JSC) is used and is defined as:

$$JSC = \frac{|\, S_{T(u)} \bigcap S_R \,|}{|\, S_{T(u)} \bigcup S_R \,|}, \tag{32}$$

where $S_{T(u)}$ and S_R represents the region of interest in the transformed template image (after registration) and reference image respectively. Fig. 17 shows that the JSC for Gaussian curvature model 1 in (12) is 0.41333 and JSC for Gaussian curvature model 2 in (14) is 0.8591 which is closer to 1 and indicates the accuracy and efficiency of the Gaussian curvature model 2 in (14) over the Gaussian curvature model 1 in (12).

F. QUANTITATIVE COMPARISON OF THE PROPOSED MODELS WITH LCMI MODEL AND LCNGF MODEL IN TERMS OF JSC

In this section the quantitative comparison of the proposed models with two other state-of-the-art models in terms of the Jaccard Similarity Coefficient is given. For comparison, two state-of-the-art models are used: Linear Curvature model using MI as similarity measure (LCMI) [45] and Linear Curvature model using NGF as similarity measure (LCNGF) [25], [45] by taking their Jaccard Similarity Coefficients (JSC). The experiments investigate the capabilities of the proposed models for image registration over the state-of-the-art models, of various MRI and synthetic noisy images of size 128×128. In Table 4 the proposed models are compared with the existing models and has produce better JSC in almost all the cases which indicates better performance of the proposed models over the existing models.

G. APPLICATION OF THE PROPOSED MODELS ON NOISY IMAGE

We have tested our proposed models on real noisy image from TEST 1 with different noise means i.e.

TABLE 4. Quantitative Comparison of LCMI model, LCNGF model and the proposed models in terms of JSC.

Images	Jaccard Similarity Coefficient(JSC)			
	LCMI	LCNGF	Proposed Model 1	Proposed Model 2
TEST1	0.7085	0.7171	0.8064	0.8106
TEST2	0.1917	0.1904	0.9185	0.9483
TEST4(T1-T2)	0.9026	0.9079	0.9288	0.9885
TEST4(T1-PD)	0.9018	0.9026	0.9199	0.9419

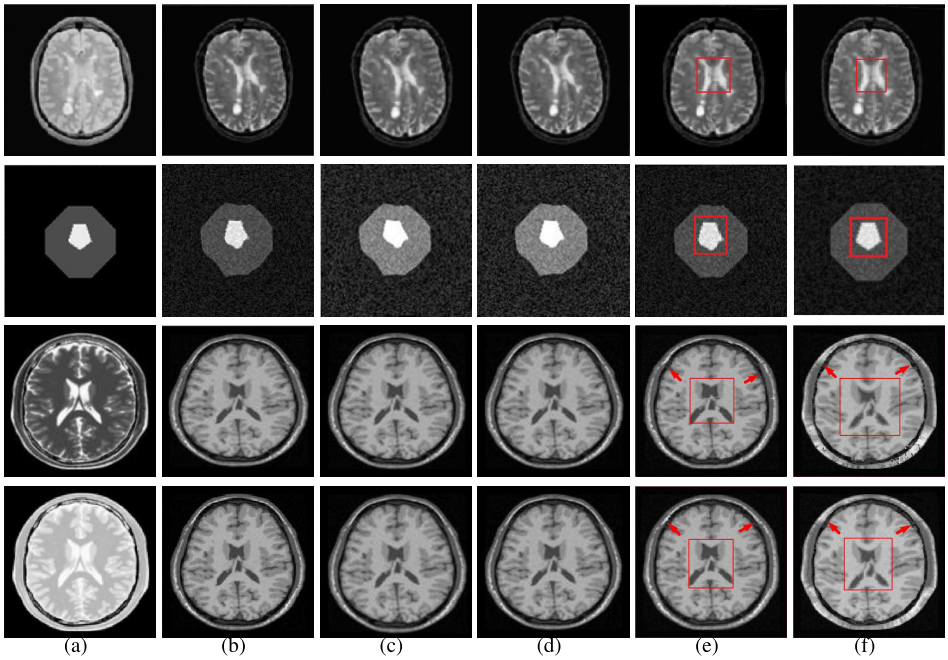

FIGURE 18. Comparison of the proposed models with state-of-the-art models by using Jaccard Similarity Coefficient. (a) R, (b) T, (c) $T(u)$ by LCMI model, (d) $T(u)$ by the LCNGF model, (e) $T(u)$ by the proposed Gaussian curvature model 1 using MI as similarity measure, (f) $T(u)$ by the proposed Gaussian curvature model 2 using NGF as similarity measure. The red square boxes and arrows on the transformed template images of the proposed models shows good registration results in all the cases.

0.03, 0.05, 0.07, 0.15, 0.2, 0.4 and variance 0.01. Fig. 19 illustrates the final registration results of the proposed models. Fig. 19 (a) shows the original reference image, 19(b) shows the original template image, from (c)-(h) shows the registered images by model in (12) using MI as similarity measure and (i)-(n) shows the registered images by model 2 in (14) using NGF as similarity measure, which are corrupted with different noise means and variance 0.01. The final registration results shows that in both the proposed models, the model 2 in (14) using NGF as similarity measure efficiently register in all images in the presence of Gaussian noise. Even for the presence of 0.4 Gaussian noise mean the model 2 using NGF is able to perform well to register, while the proposed model 1 in (12) using MI as similarity measure is efficient up to mean 0.20 and variance 0.01.

To quantitatively evaluate the accuracy of the registration algorithms, the correlation coefficients between the reference and transformed template images are compared. The correlation coefficient $\rho(T(u), R)$ between the transformed template image $T(u)$ and reference image R is given by:

$$\rho(T(u), R) = \frac{\sum_m \sum_n \left(T(u)_{mn} - \bar{T(u)}\right)\left(R_{mn} - \bar{R}\right)}{\sqrt{\sum_m \sum_n \left(T(u)_{mn} - \bar{T(u)}\right)^2 \left(R_{mn} - \bar{R}\right)^2}}, \tag{33}$$

where $T(u)$ and R are m $\times$ n are two-dimensional images and $\bar{T(u)}$ and $\bar{R}$ represent the mean value of the elements of $T(u)$ and R, respectively. A correlation coefficient of zero indicates a low degree of matching between the images, and a Correlation Coefficient of 1 indicates exact similarity between the images. Correlation Coefficients are a commonly used representation of similarity between images for the evaluation of deformable registration techniques.

The statistical analysis of the noise added image is done in Table 5, which shows that the proposed model using NGF can efficiently work upto mean 0.04 and variance 0.01, while the proposed model using MI as similarity measure is efficient upto mean 0.20 and variance 0.01. Also to quantitatively

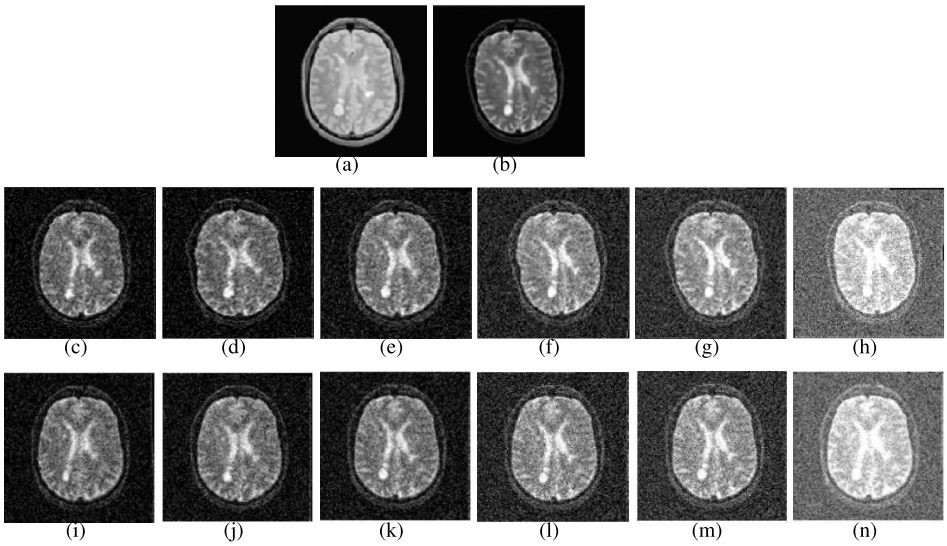

FIGURE 19. Final registration results of real noisy medical image by the proposed models (a) Original Reference image (b) Original Template image and (c-h) transformed template images with Gaussian noise by proposed model 1 using MI as similarity measure and (i-n) transformed template images with Gaussian noise by proposed model 2 using NGF as similarity measure of different means 0.03, 0.05, 0.07, 0.15, 0.2, 0.4 and variance 0.01, respectively.

TABLE 5. Comparison of the proposed models using MI and NGF as similarity measures using coefficient of correlation by adding Gaussian noise with different Means and Variance = 0.01.

Means	0.03	0.05	0.07	0.15	0.2	0.4
Coefficient of Correlation for the proposed model 1 using MI	0.9	0.89	0.88	0.85	0.84	0.65
Coefficient of Correlation for the proposed model 2 using NGF	0.95	0.93	0.89	0.88	0.87	0.74

evaluate the accuracy of the proposed models the correlation coefficient between the reference and template images are compared. The results produced in Table 5 and Fig. 19 demonstrate that the proposed Gaussian curvature model 2 in (14) using NGF as similarity measure is a significant improvement over the Gaussian curvature model 1 in (12) using MI as similarity measure.

V. CONCLUSION

In this paper, we proposed two non-rigid image registration models for the alignment of multi-modality images. In these models, we have shown that the Gaussian curvature is incorporated as regularization term with mutual information and normalized gradient field, which are used as the data terms to measure the similarity of the multi-modality images to be registered. In order to solve the proposed registration models efficiently, we used Augmented Lagrangian method for its numerical implementation. The proposed models can register multi-modality images without effecting edges and other important fine details. The proposed models produce good registration results in multi-modality images such as medical and synthetic images as compared to the existing state of the art models quantitatively. Experimental results of the proposed registration models shows that the registered template images are very similar to the reference images and exhibits an excellent registration performance with better values of the Jaccard similarity coefficient. Moreover, they are tested on MR images taken from the free available database Brainweb in order to get better registration results. To quantitatively evaluate the accuracy of the proposed models the correlation coefficient between the reference and template images are compared. The results demonstrate that the proposed Gaussian curvature model 2 using NGF as similarity measure has a significant improvement over the proposed model 1 using MI as similarity measure. The proposed models with Gaussian curvature works better for the large and smooth deformations without mesh folding while existing models with linear curvature may not produce better results for large deformations and may produce mesh folding. The only limitation of the proposed models is that they are computationally costly and needs high processors systems. Future work could investigate options for further improvements. It can be expected that the models can be applied to the real data sets of multi-modality images. Also, the proposed models can be apply to high resolution multi-modality images.

REFERENCES

[1] F. P. M. Oliveira and J. M. R. S. Tavares, "Medical image registration: A review," *Comput. Methods Biomech. Biomed. Eng.*, vol. 17, no. 2, pp. 73–93, 2014.

[2] A. Sotiras, C. Davatzikos, and N. Paragios, "Deformable medical image registration: A survey," *IEEE Trans. Med. Imag.*, vol. 32, no. 7, pp. 1153–1190, Jul. 2013.

[3] P. Campisi and K. Egiazarian, *Blind Image Deconvolution: Theory and Applications*. Boca Raton, FL, USA: CRC Press, 2016.
[4] F. Alam, S. U. Rahman, A. U. Din, and F. Qayum, "Medical image registration: Classification, applications and issues," *J. Postgraduate Med. Inst.*, vol. 32, pp. 1–8, Nov. 2018.
[5] Z. Nie and X. Yang, "Deformable image registration using functions of bounded deformation," *IEEE Trans. Med. Imag.*, vol. 38, no. 6, pp. 1488–1500, Jun. 2019.
[6] B. Fischer and J. Modersitzki, "Fast diffusion registration," in *Contemporary Mathematics*, vol. 313. Providence, RI, USA: American Mathematical Society, 2002, pp. 117–128.
[7] T. Thompson and K. Chen, "A more robust multigrid algorithm for diffusion type registration models," *J. Comput. Appl. Math.*, vol. 361, pp. 502–527, Dec. 2019.
[8] N. Chumchob, "Vectorial total variation-based regularization for variational image registration," *IEEE Trans. Image Process.*, vol. 22, no. 11, pp. 4551–4559, Nov. 2013.
[9] W. Hu, Y. Xie, L. Li, and W. Zhang, "A total variation based nonrigid image registration by combining parametric and non-parametric transformation models," *Neurocomputing*, vol. 144, pp. 222–237, Nov. 2014.
[10] C. Broit, "Optimal registration of deformed images," Ph.D. dissertation, Univ. Pennsylvania, Philadelphia, PA, USA, 1981.
[11] B. Fischer and J. Modersitzki, "Curvature based image registration," *J. Math. Imag. Vis.*, vol. 18, no. 1, pp. 81–85, 2003.
[12] N. Chumchob and K. Chen, "Improved variational image registration model and a fast algorithm for its numerical approximation," *Numer. Methods Partial Differ. Equ.*, vol. 28, no. 6, pp. 1966–1995, Nov. 2012.
[13] N. Chumchob, K. Chen, and C. Brito-Loeza, "A fourth-order variational image registration model and its fast multigrid algorithm," *Multiscale Model. Simul.*, vol. 9, no. 1, pp. 89–128, Jan. 2011.
[14] M. Ibrahim, K. Chen, and C. Brito-Loeza, "A novel variational model for image registration using Gaussian curvature," 2015, *arXiv:1504.07643*. [Online]. Available: http://arxiv.org/abs/1504.07643
[15] J. Modersitzki, *FAIR: Flexible Algorithms for Image Registration*. Philadelphia, PA, USA: SIAM, 2009.
[16] J. Feydy, B. Charlier, F. X. Vialard, and G. Peyre, "Optimal transport for diffeomorphic registration," in *Proc. Int. Conf. Med. Image Comput. Comput.-Assist. Intervent.*, 2017, pp. 291–299.
[17] Y. He, A. B. Hamza, and H. Krim, "A generalized divergence measure for robust image registration," *IEEE Trans. Signal Process.*, vol. 51, no. 5, pp. 1211–1220, May 2003.
[18] C. Guetter, C. Xu, F. Sauer, and J. Hornegger, "Learning based non-rigid multi-modal image registration using Kullback-Leibler divergence," in *Proc. Int. Conf. Med. Image Comput. Comput.-Assist. Intervent.*, 2005, pp. 255–262.
[19] F. Wang, B. C. Vemuri, M. Rao, and Y. Chen, "Cumulative residual entropy, a new measure of information & its application to image alignment," in *Proc. 9th IEEE Int. Conf. Comput. Vis.*, Oct. 2003, p. 548.
[20] C. Studholme, D. L. G. Hill, and D. J. Hawkes, "An overlap invariant entropy measure of 3D medical image alignment," *Pattern Recognit.*, vol. 32, no. 1, pp. 71–86, Jan. 1999.
[21] S. Wu, P. He, S. Yu, S. Zhou, J. Xia, and Y. Xie, "To align multimodal lumbar spine images via bending energy constrained normalized mutual information," *BioMed Res. Int.*, vol. 2020, pp. 1–11, Jul. 2020.
[22] A. Collignon, F. Maes, D. Delaere, D. Vandermeulen, P. Suetens, and G. Marchal, "Automated multi-modality image registration based on information theory," *Inf. Process. Med. Imag.*, vol. 6, pp. 263–274, Jun. 1995.
[23] P. Viola and W. M. Wells, III, "Alignment by maximization of mutual information," *Int. J. Comput. Vis.*, vol. 24, no. 2, pp. 137–154, Sep. 1997.
[24] W. M. Wells, III, P. Viola, H. Atsumi, S. Nakajima, and R. Kikinis, "Multi-modal volume registration by maximization of mutual information," *Med. Image Anal.*, vol. 1, pp. 35–51, Mar. 1996.
[25] E. Haber and J. Modersitzki, "Intensity gradient based registration and fusion of multi-modal images," in *Proc. Int. Conf. Med. Image Comput. Comput.-Assist. Intervent.*, 2006, pp. 726–733.
[26] E. Hodneland, A. Lundervold, J. Rørvik, and A. Z. Munthe-Kaas, "Normalized gradient fields for nonlinear motion correction of DCE-MRI time series," *Comput. Med. Imag. Graph.*, vol. 38, no. 3, pp. 202–210, Apr. 2014.
[27] Y. Chen, J. Shi, M. Rao, and J.-S. Lee, "Deformable multi-modal image registration by maximizing Renyi's statistical dependence measure," *Inverse Problems Imag.*, vol. 9, no. 1, pp. 79–103, 2015.
[28] M. Ibrahim and K. Chen, "Multi-modality image registration using the decomposition model," *AIP Conf.*, vol. 1830, p. 02007, Apr. 2017.
[29] K. Brehmer, H. O. Aggrawal, S. Heldmann, and J. Modersitzki, "Variational registration of multiple images with the SVD based S_qN distance measure," in *Proc. Int. Conf. Scale Space Variational Methods Comput. Vis.*, 2019, pp. 251–262.
[30] A. Theljani and K. Chen, "An augmented Lagrangian method for solving a new variational model based on gradients similarity measures and high order regulariation for multimodality registration," *Inverse Problems Imag.*, vol. 13, no. 2, pp. 309–335, 2019.
[31] T. M. Cover and J. A. Thomas, *Elements of Information Theory*, vol. 68. New York, NY, USA: Wiley, 1991, pp. 69–73.
[32] I. Vajda, *Theory of Statistical Inference and Information*, vol. 11. The Hague, The Netherlands: Kluwer, 1989.
[33] F. Maes, A. Collignon, D. Vandermeulen, G. Marchal, and P. Suetens, "Multimodality image registration by maximization of mutual information," *IEEE Trans. Med. Imag.*, vol. 16, no. 2, pp. 187–198, 1997.
[34] S. Heldmann, O. Mahnke, D. Potts, J. Modersitzki, and B. Fischer, "Fast computation of mutual information in a variational image registration approach," in *Bildverarbeitung fur die Medizin*. Berlin, Germany: Springer, 2004, pp. 448–452.
[35] X. Huang, "Nonrigid image registration problem using fluid dynamics and mutual information," *J. Biometrics Biostatistics*, vol. 12, p. 1, Jan. 2014.
[36] E. D. Agostino, F. Maes, D. Vandermeulen, and P. Suetens, "A viscous fluid model for multimodal non-rigid image registration using mutual information," in *Proc. Int. Conf. Med. Image Comput. Comput.-Assist. Intervent.*, 2002, pp. 541–548.
[37] E. Parzen, "On estimation of a probability density function and mode," *Ann. Math. Statist.*, vol. 33, no. 3, pp. 1065–1076, Sep. 1962.
[38] R. O. Duda and P. E. Hart, *Pattern Classification and Scene Analysis*. New York, NY, USA: Wiley, 1973.
[39] R. Xu, Y.-W. Chen, S.-Y. Tang, S. Morikawa, and Y. Kurumi, "Parzen-window based normalized mutual information for medical image registration," *IEICE Trans. Inf. Syst.*, vol. E91-D, no. 1, pp. 132–144, Jan. 2008.
[40] E. Haber and J. Modersitzki, "Beyond mutual information: A simple and robust alternative," in *Bildverarbeitung fur die Medizin*. Berlin, Germany: Springer, 2005, pp. 350–354.
[41] M. Ibrahim, "Variational models and numerical algorithms for effective image registration," Ph.D. dissertation, Univ. Liverpool, Liverpool, U.K., 2015.
[42] C. Brito-Loeza, K. Chen, and V. Uc-Cetina, "Image denoising using the Gaussian curvature of the image surface," *Numer. Methods Partial Differ. Equ.*, vol. 32, no. 3, pp. 1066–1089, May 2016.
[43] A. Myronenko and X. Song, "Intensity-based image registration by minimizing residual complexity," *IEEE Trans. Med. Imag.*, vol. 29, no. 11, pp. 1882–1891, Nov. 2010.
[44] *Brainweb: Simulated Brain Database*. Accessed: Aug. 2020. [Online]. Available: http://www.bic.mni.mcgill.ca/brainweb
[45] B. Fischer and J. Modersitzki, "FLIRT: A flexible image registration toolbox," in *Proc. Int. Workshop Biomed. Image Registration*, 2003, pp. 261–270.

NASRA BEGUM received the master's degree in mathematics from the University of Peshawar, Pakistan, in 2002, and the M.Phil. degree in mathematics from Shaheed Benazir Bhutto Women University, Peshawar, Pakistan, in 2015. She is currently pursuing the Ph.D. degree with the Department of Basic Sciences and Islamiat, University of Engineering and Technology, Peshawar, Peshawar. She is also working as a Lecturer with the Department of Mathematics, Shaheed Benazir Bhutto Women University. Her current research interests include image processing, image registration, and computational mathematics.

NOOR BADSHAH received the Ph.D. degree in mathematics from the University of Liverpool, U.K. He is currently working as an Associate Professor with the Department of Basic Science, University of Engineering and Technology, Peshawar, Pakistan. His current research interests include modeling in image processing, biology, and computational mathematics.

MAZLINDA IBRAHIM received the Ph.D. degree in mathematics from the University of Liverpool, U.K., in 2015. She is currently working as a Senior Lecturer with the National Defense University of Malaysia. Her current research interests include modeling in image processing and computational mathematics.

MUNIBA ASHFAQ received the B.S. and M.S. degrees in computer systems engineering from the University of Engineering and Technology, Peshawar, Pakistan, in 2008 and 2013, respectively, where she is currently pursuing the Ph.D. degree in computer systems engineering. She is also serving as a Lecturer for the Department of Computer Systems Engineering, University of Engineering and Technology, Peshawar. Her research interests include biomedical image processing and analysis for disease detection and segmentation (brain tumor, multiple sclerosis, and skin cancer) using machine learning and image registration techniques, 3D shape measurement, parallel processing, image compression, and object recognition and classification.

NASRU MINALLAH received the B.Sc. degree in computer engineering from the University of Engineering and Technology, Peshawar, Pakistan, in 2004, the M.Sc. degree in computer engineering from the Lahore University of Management Sciences, Lahore, Pakistan, in 2006, and the Ph.D. degree from the Communications Group, School of Electronics and Computer Science, University of Southampton, Southampton, U.K., in 2010. He is currently working as an Associate Professor with the Department of Computer Systems Engineering, University of Engineering and Technology, Peshawar. His research interests include image processing, remote sensing, low-bit-rate video coding for wireless communications, turbo coding and detection, and iterative source-channel decoding.

HADIA ATTA received the M.Sc. degree in mathematics from Shaheed Benazir Bhutto Women University, Peshawar, Pakistan, in 2008, and the M.S. degree in mathematics from the University of Engineering and Technology, Peshawar, Peshawar, in 2014. She is currently pursuing the Ph.D. degree with the Department of Mathematics, Islamia College Peshawar, Pakistan. Her current research interests include image processing, image segmentation, and computational mathematics.